Available online at www.sciencedirect.com
SCIENCE DIRECT®
Thin Solid Films 450 (2004) 216–221
thin solid films
www.elsevier.com/locate/tsf

# Anisotropic crystallite size analysis of textured nanocrystalline silicon thin films probed by X-ray diffraction

M. Morales[a,*], Y. Leconte[a], R. Rizk[a], D. Chateigner[b]

[a]*Laboratoire d'Etudes et de Recherche sur les Matériaux-ENSICAEN, 6 Bd. du Maréchal Juin, F-14050 Caen, France*
[b]*Laboratoire de Cristallographie et Sciences des Matériaux-ENSICAEN, F-14050 Caen, France*

**Abstract**

A newly developed X-ray technique is used, which is able to quantitatively combine texture, structure, anisotropic crystallite shape and film thickness analyses of nanocrystalline silicon films. The films are grown by reactive magnetron sputtering in a plasma mixture of $H_2$ and Ar onto amorphous $SiO_2$ and single-crystal (100)-Si substrates. Whatever the used substrate, preferred orientations are observed with texture strengths around 2–3 times a random distribution, with a tendency to achieve lower strengths for films grown on $SiO_2$ substrates. As a global trend, anisotropic shapes and textures are correlated with longest crystallite sizes along the ⟨111⟩ direction but absence of ⟨111⟩ oriented crystallites. Cell parameters are systematically observed larger than the value for bulk silicon, by approximately 0.005–0.015 Å.


*Keywords:* Silicon; Sputtering; X-Ray diffraction; Anisotropy; Texture analysis

## 1. Introduction

A large number of studies is devoted nowadays to nanocrystalline silicon thin films as promising structures for flat panel display applications [1]. For these large area microelectronic applications, the current trend is to lower the process temperature to enable the use of low cost substrates such as common glasses and flexible polymers. Crystallised silicon layers have recently been achieved at relatively low temperature by synchrotron-radiation decomposition of disilane [2], by plasma enhanced chemical vapour deposition (PECVD) [3] and also by our group using reactive magnetron sputtering (RMS) [4]. Most of the films produced by PECVD and RMS techniques consist of a mixture of amorphous and crystalline silicon, obtained through the interactions between the growing surface and the reactive hydride radicals present in the hydrogen-rich plasma. The growth and crystallization mechanisms are still a matter of debate [5,6], even though the key role of the highly reactive hydride species is now described by about three models [7,8]. In our case, these mechanisms lead to the simultaneous stabilisation of crystallite preferential orientations (texture) and anisotropic crystallite shapes, and are associated to cell parameter variations. For the first time, we used in this work a newly developed X-ray technique, which is able to combine quantitatively the texture, structure and anisotropic shape determination.

## 2. Samples and experiments

Silicon thin films were grown by RMS in a plasma mixture of $H_2$ and Ar at 200 °C on amorphous $SiO_2$ (a-$SiO_2$) and single-crystal (100)-Si substrates. The deposition conditions were the following: power density 2 W/cm$^2$, total pressure of $10^{-1}$ Torr, 80% of hydrogen partial pressure. For both kinds of substrates we varied the target–substrate distance ($d$). For a-$SiO_2$ substrates the $d$ values were 4, 6, 7, 8, 10 and 12 cm corresponding to Samples A, B, C, D, E and F, respectively, while on (100)-Si two typical $d$ values were chosen, $d=6$ and 12 cm (Samples G and H, respectively), aiming the comparison of the substrate effect.

The structural characteristics of the films were carefully characterised by X-ray diffraction (XRD) while their optical properties were examined by optical transmission spectroscopy performed on a Perkin–Elmer UV/VIS (from 0.4 to 4.1 eV). As the XRD patterns of

*Corresponding author. Tel.: +33-2-31-45-26-58; fax: +33-2-31-45-26-60.
*E-mail address:* magali.morales@ismra.fr (M. Morales).

0040-6090/04/$ - see front matter © 2003 Elsevier B.V. All rights reserved.
doi:10.1016/j.tsf.2003.10.074

the corresponding thin films exhibited preferential orientations and anisotropic line broadening, X-ray quantitative texture analysis (QTA) was performed, with a simultaneous Rietveld refinement including anisotropic line broadening and film thickness analyses. We used a Huber 4-circles diffractometer and a curved position sensitive detector (INEL CPS 120), which spans a 120° range in $2\theta$, allowing the simultaneous acquisition of several pole figures. These latter were measured by scanning the tilt angle of the goniometer, $\chi$, in the range 0–60° and the azimuthal angle, $\varphi$, in the range 0–360°, both using a 5° step with an incident X-ray beam $\omega = 14.2°$ corresponding to the Bragg angle of the 111 reflection of the silicon.

For the treatment of these X-ray diffractograms, we used the material analysis using diffraction (MAUD) program [9] that combines the WIMV method [10], used to solve the orientation distribution function (ODF), with a Rietveld analysis to extract the microstructural and structural parameters. The integrated intensities, extracted by the Le Bail method, are treated and corrected for the absorption, volume variations and delocalisation effects [11]. The instrumental resolution function has been determined by a full mapping (in $\omega$, $\chi$ and $2\theta$ ranges) of our diffractometer space using the NIST $LaB_6$ powder standard [12] used for the International crystallographic round-robin. The (hkl) dependence of diffraction line broadening are determined in the program by the use of the Popa rules based on the symmetrised spherical harmonics to describe the crystallite shape model [13]. The thin film thicknesses are additional parameters refined during the Rietveld refinement, implemented in the MAUD package via the necessary intensity corrections [14]. These thicknesses are compared to those obtained by profilometry (Dektak3 ST). The pole figures are normalised into distribution densities that are expressed as multiples of a random distribution (m.r.d.). The ODF allows then the recalculation of the experimental pole figures for comparison with the observed data and first reliability evaluation. The statistical ODF reliability is evaluated by calculation of the reliability factors $RP_0$ [15], and the overall texture strength is estimated by the texture index, $F^2$, value [16]. Since our observed textures are axially symmetric around the normal to the film plane (fibre textures), the inverse pole figure calculated for this normal direction (**001**) is a complete representation of the ODF. We then choose to illustrate the exhibited textures using such inverse pole figures. Data reduction and calculations of the inverse pole figures were operated using the Goman, Pofint [17] and Beartex [18] packages, respectively.

## 3. Results and discussion

A typical XRD pattern of the obtained silicon thin films is shown in Fig. 1, for sample D ($d = 8$ cm). A pure silicon phase is observed for all samples, indexed in the regular diamond cubic structure of Si, with cell parameters around 5.44 Å (Table 1), always refined larger than the value for bulk silicon by approximately 0.005–0.015 Å. A strong and anisotropic broadening of the diffracted lines is observed due to anisotropic shapes of individual crystallites. Whatever the deposition conditions and the substrate, the mean crystallite shape corresponds to an ellipsoid elongated along the [111] direction and almost isotropic in perpendicular directions. As illustrated for Sample D in Fig. 2, the crystallite average size along [111] is around 90 Å and 30–40 Å in the perpendicular directions. We could not detect neither significant Gaussian contribution in any of the peaks (no microstrains are present) in our films nor could any peak shift be detected when tilting the samples (no residual stress is stabilised). The film's thickness is approximately 1460 nm and the thicknesses refined by XRD are systematically observed smaller than the ones measured by profilometry for $d > 4$ cm (Table 2). For sample A, it was not possible to refine the film thickness, which was fixed to 7080 Å (value measured by profilometry) for the refinement. These films, deposited close to the cathode, were found relatively thin because of the low values of the deposition rate encountered in this region where a strong formation of Si nanopowder is observed. This formation leads to the consumption of the highly sticking $SiH_2$ radicals that are no more available for the growth of the film [19]. For Samples B and C, the X-ray refined thicknesses are around half of the profilometry ones whereas for samples D–H, this difference is smaller. This is attributed either to the film's porosity or/and to the curvature of the films surface, with smaller thicknesses towards the edge of the samples. This latter hypothesis is coherent with the observation of Newton rings under visible light, located on the periphery of the disc-shaped layers.

However, such an XRD pattern is typical of a textured sample, with peak ratios different from the ones of the powder. A selected set of diffraction diagrams shows an example of peak variations due to texture when the sample is tilted in $\chi$ (Fig. 1). The simulated diagrams for every $\chi$ position is also shown and attest for the goodness of the refinement, when all parameters are taken into account (texture, microstructure, cell parameters, thickness, anisotropic crystallite sizes), and as denoted by the reliability factors not exceeding 5.5% (Table 1).

Films deposited on a-$SiO_2$ substrates show large texture dependence with inter-electrode distance. If the overall texture strength of the films appears almost unaffected by the $d$ variation (with $F^2$ around 1.2 m.r.d.$^2$ at maximum and **001** inverse pole figure maxima not larger than 2 m.r.d.), the resulting texture components are strongly influenced (Fig. 3). The closest distance (Sample A) favours an orientation with ⟨110⟩

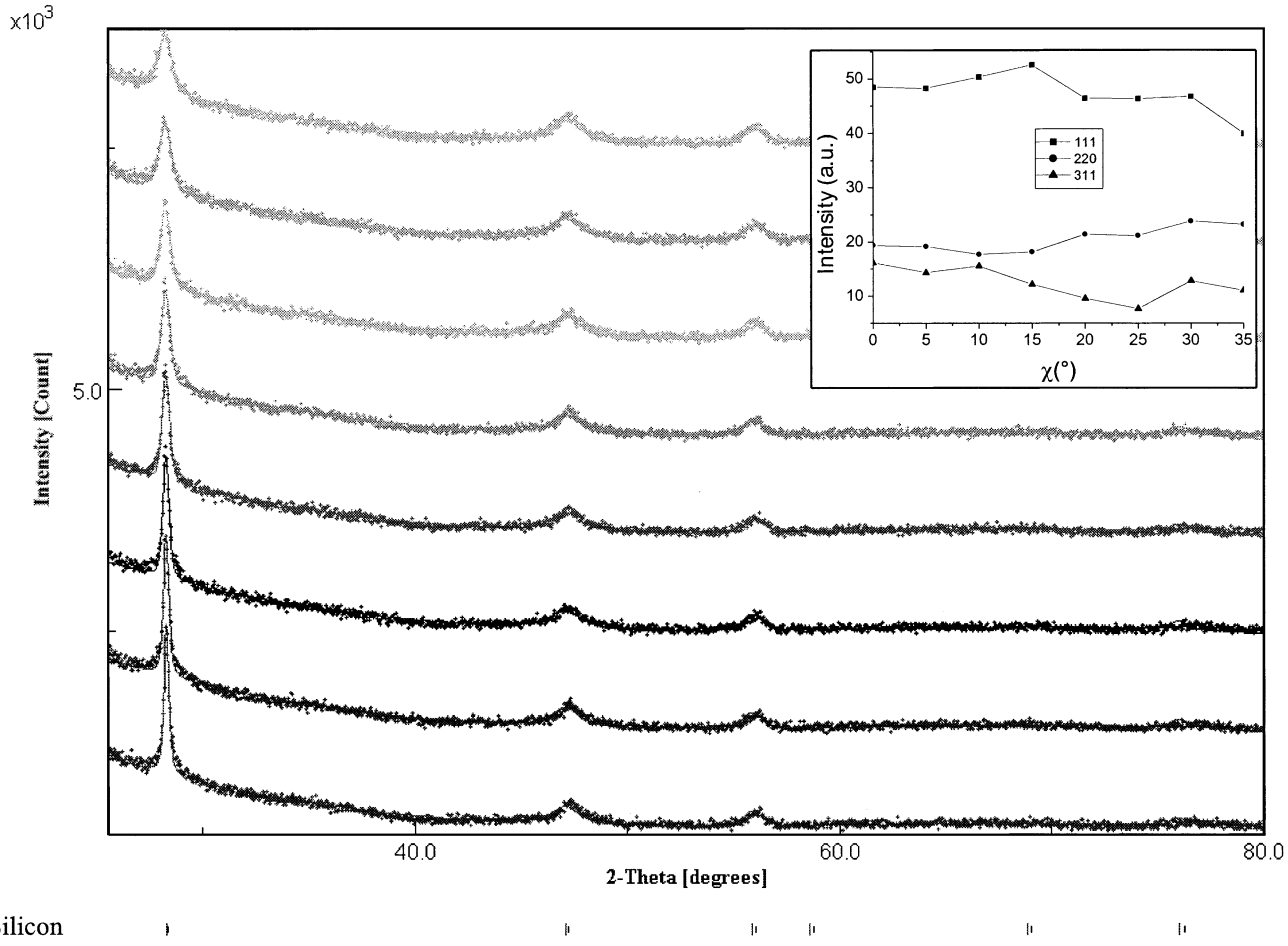


Fig. 1. Typical XRD diagram measured (dotted line) on Sample D ($d=8$ cm) at different $\chi$ positions ($\chi=0$ at bottom and $\chi=35°$ at top) showing the broad and anisotropic diffracted lines, and the corresponding simulated spectra (solid line). Insert shows the texture presence by the $\chi$-scans of the three main integrated intensities (background is subtracted). Note the particularly high 311 intensity and the non-constant variations of the lines with $\chi$.

directions aligned with the films normal as a major texture component (Fig. 3). But minor components with ⟨100⟩ and ⟨124⟩ directions of crystallites along the normal are also observed in this film. The ⟨110⟩ orientation is destabilised for distances larger than 4 cm, and does not exist anymore for $d=6$ cm (Sample B). This ⟨110⟩ component removal is accompanied by a slight tilt of the ⟨100⟩ (which could correspond to a ⟨h0$l$⟩ alignment with $l$ approx. 10–11) and the appearance of a large component centred on ⟨221⟩ like

Table 1
List of structural and microstructural parameters of the films resulting from the refinement and associated reliability factors $R$ ($R_w$: weighted, $R_B$: Bragg, $R_{exp}$: experimental, $RP_0$: ODF factor for all distribution densities). Numbers in parentheses represent errors on the last digit

| Sample | $d$ (cm) | $a$ (Å) | RX thickness (nm) | Anisotropic sizes (Å) | | | Texture parameters | | | Reliability factors (%) | | | |
|---|---|---|---|---|---|---|---|---|---|---|---|---|---|
| | | | | ⟨111⟩ | ⟨220⟩ | ⟨311⟩ | Maximum (m.r.d.) | Minimum (m.r.d.) | Texture index $F^2$ (m.r.d.$^2$) | $RP_0$ | $R_w$ | $R_B$ | $R_{exp}$ |
| A | 4 | 5.4466 (3) | – | 94 | 20 | 27 | 1.95 | 0.4 | 1.12 | 1.72 | 4.0 | 3.7 | 3.5 |
| B | 6 | 5.4439 (2) | 711 (50) | 101 | 20 | 22 | 1.39 | 0.79 | 1.01 | 0.71 | 4.9 | 4.3 | 4.2 |
| C | 7 | 5.4346 (4) | 519 (60) | 99 | 40 | 52 | 1.72 | 0.66 | 1.05 | 0.78 | 4.3 | 4.0 | 3.9 |
| D | 8 | 5.4461 (2) | 1447 (66) | 100 | 22 | 33 | 1.57 | 0.63 | 1.04 | 0.90 | 5.5 | 4.6 | 4.5 |
| E | 10 | 5.4462 (2) | 1360 (80) | 98 | 20 | 25 | 1.22 | 0.82 | 1.01 | 0.56 | 5.0 | 3.9 | 4.0 |
| F | 12 | 5.4452 (3) | 1110 (57) | 85 | 22 | 26 | 1.59 | 0.45 | 1.05 | 1.08 | 4.2 | 3.5 | 3.7 |
| G | 6 | 5.4387 (3) | 1307 (50) | 89 | 22 | 28 | 1.84 | 0.71 | 1.01 | 1.57 | 5.2 | 4.7 | 4.2 |
| H | 12 | 5.4434 (2) | 1214 (18) | 88 | 22 | 24 | 2.77 | 0.50 | 1.12 | 2.97 | 5.0 | 4.5 | 4.3 |

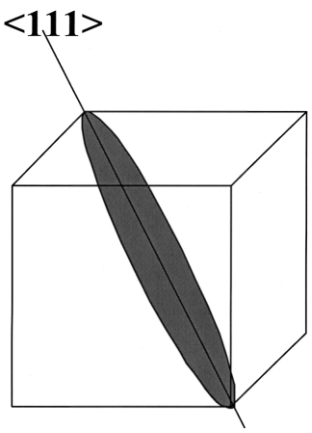


Fig. 2. Schematic mean crystallite shape for Sample D represented in a cubic cell, as refined using the Popa approach and exhibiting a strong elongation along ⟨111⟩.

Table 2
Comparison of the film thicknesses determined by X-ray diffraction (RX) and profilometry

| Samples | *d* (cm) | Profilometry thickness (nm) | RX thickness (nm) |
|---|---|---|---|
| A | 4 | 708 | – |
| B | 6 | 1350 | 711 (50) |
| C | 7 | 1530 | 519 (60) |
| D | 8 | 1465 | 1447 (66) |
| E | 10 | 1470 | 1360 (80) |
| F | 12 | 1208 | 1110 (57) |
| G | 6 | 1350 | 1307 (50) |
| H | 12 | 1200 | 1214 (18) |

orientation. Since this component is largely distributed, it corresponds to a set of closely oriented directions like ⟨332⟩, ⟨443⟩, ⟨554⟩… that can be present in this film too. An interesting behaviour is the progressive shift of this latter component towards a ⟨111⟩ position for increasing distances (Samples B–F). Comparing films B and F, one clearly sees the general trend starting in B

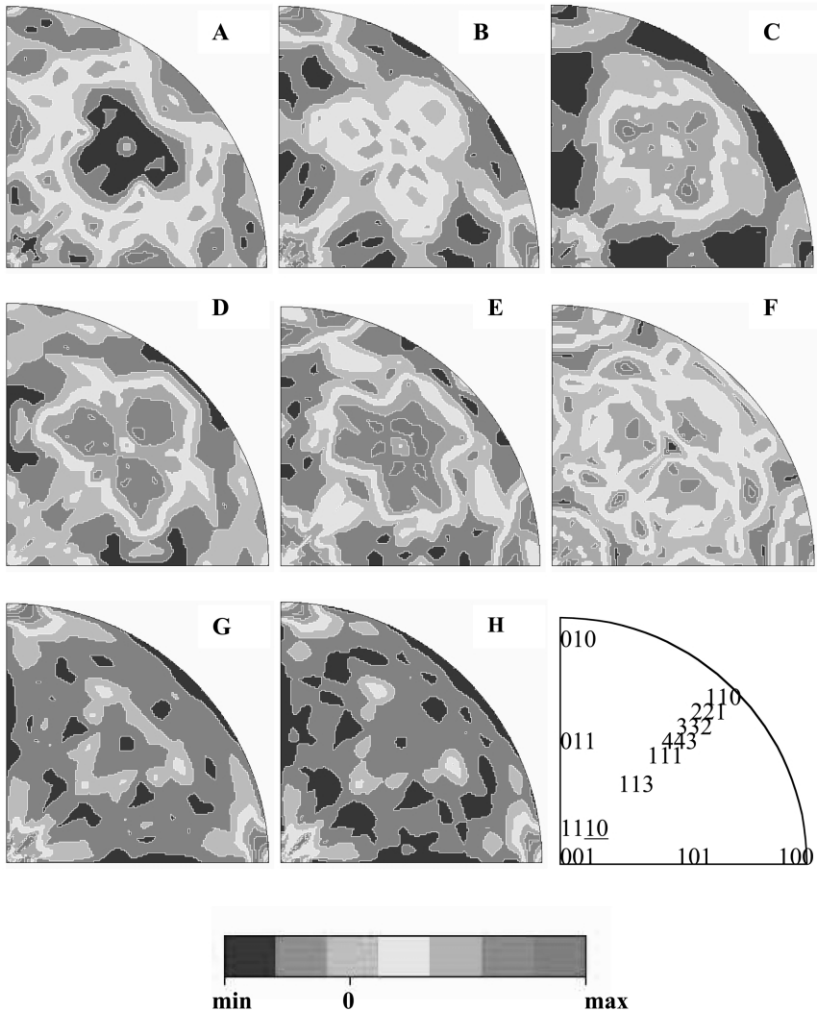


Fig. 3. **001** inverse pole figures for samples deposited on a-$SiO_2$ (Sample A–F) and on (100)-Si (Sample G and H). Pole locations are indicated by their Miller indices (bottom right) equal area projections, linear distribution density scale.

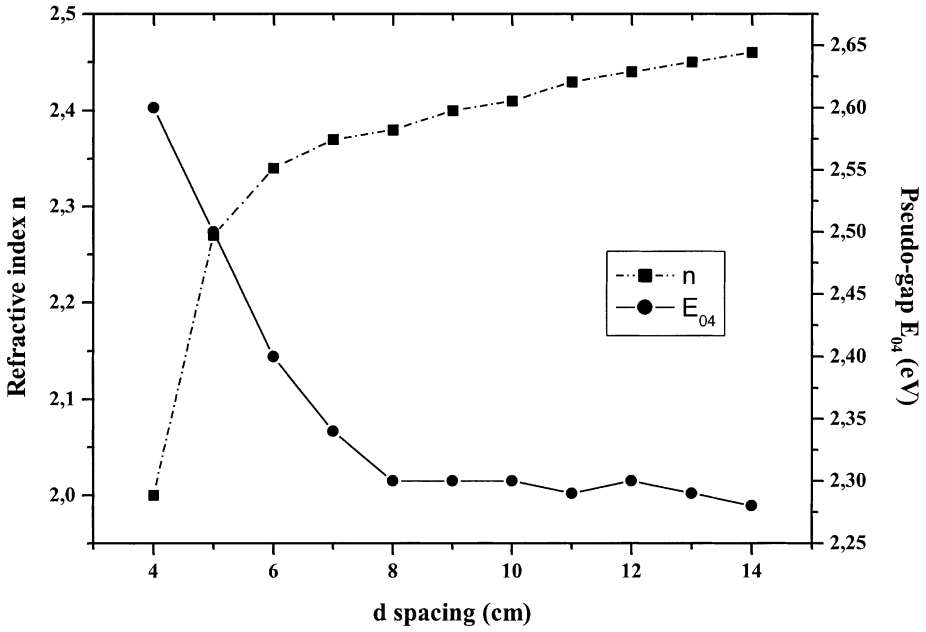


Fig. 4. Evolution of the refractive index $n$ and of the pseudo-gap $E_{04}$ with the distance $d$. Lines are only guides for eyes.

from orientations around ⟨221⟩, and reaching ⟨443⟩ or ⟨553⟩ in F. However, if the texture component would tend to coincide with a ⟨111⟩ orientation for largest $d$'s (that is along the highest dimension of the crystallites), no pure ⟨111⟩ orientation is observed, that would correspond to a favoured growth at the bulk state in such structures, as in diamond thin films for instance [20]. The ⟨100⟩ inclined orientation is fully removed for intermediate distances (Samples C and D), then reappears for larger distances up to 12 cm.

Whatever the distance used, using (100)-Si single crystals as substrates strongly stabilises the ⟨100⟩ orientation (Fig. 3). This orientation corresponds to the heteroepitaxial component with [100] directions of the film aligned with the ones of the substrate. The formation of native amorphous $SiO_2$ layer at the surface of the substrate would imply a growth mechanism similar to that observed on a-$SiO_2$. However, this native oxide is etched by the hydrogen species present in the plasma during deposition leading to a growth directly onto a bare silicon single crystal surface.

Whatever the substrate no ⟨111⟩ texture could be observed, but a systematic elongation of the crystallites along this direction. This apparent absence of correlation between orientation and crystal shapes is the consequence of the growth interruption induced by the fabrication process, preventing more regular growth schemes to occur like in columnar or heteroepitaxial growing. However, looking closer at mean crystal sizes along ⟨111⟩ and ⟨220⟩ directions, one observes that films in which the ⟨100⟩ orientation is present show a smaller anisotropy of their crystal shape. On (100)-Si substrates exhibiting a strong ⟨100⟩ orientation, but also for film F on a-$SiO_2$, the ⟨111⟩ mean dimension is around 87 Å, while that along ⟨220⟩ is around 22 Å. Sample A exhibiting a major ⟨110⟩ orientation but still a minor ⟨100⟩ shows ⟨111⟩ mean dimension around 94 Å, at least 5 Å less than films without the ⟨100⟩ component (Samples B, C, D and E).

The minimum values of the ODF (Table 1) are relatively high, from 0.4 to 0.82 m.r.d. This means that 40–82% of the volume of the material is randomly oriented (not textured). Any anisotropic properties than one could observe on such materials will then be the consequence of only 60–18% of the total volume, hereby considerably decreasing the probability of observation of such anisotropy.

To correlate the structural characteristics reported so far to some physical properties, optical absorption measurements were performed on our samples. Fig. 4 reports the evolution in function of the $d$ distance of both the refractive index $n$ and the pseudo-gap $E_{04}$, defined as the energy value for which the absorption coefficient $\alpha$ is equal to $10^4$ $cm^{-1}$. The refractive index shows an abrupt increase for the first stages of electrode distancing before some tendency to saturate for higher values of $d$. This behaviour would consistently reflect the evolution of the film compactness considering that the porosity of the film is increasingly higher when the deposition is performed at closer and closer distance of $d=4$ cm, as stated above from XRD analyses. This is supported by the nearly opposite evolution of $E_{04}$ since their high values for films obtained with low $d$ could originate from the relatively high density of microcavities inherent

to the film porosity. In this respect, we closely correlate the abrupt and the subsequent smooth decrease of $E_{04}$ to a similar behaviour of the film porosity, i.e. to the density of the microcavities present in our films.

## 4. Conclusions

Preferred orientations, cell parameters and anisotropic crystallite sizes of nanocrystalline silicon thin films deposited on amorphous silica and silicon single-crystal substrates have been quantitatively determined. Strong texture variations are observed when the electrode distance and/or the substrate is varied. Texture variations are correlated to the anisotropic crystal growth. The unit cell parameter of the silicon structure is always larger in the nanocrystalline films than in bulk silicon, with no apparent regular variation vs. texture or crystal growth.

## References

[1] 19th International Conference on Amorphous and Microscrystalline Semiconductors, Nice, France, August 2001, J. Non-Cryst. Solids (2002) 299–302.
[2] H. Akazawa, Phys. Rev. B 59 (1999) 3184.
[3] P. Roca, I. Cabarrocas, J. Non-Cryst. Solids 266–269 (2000) 31.
[4] Y. Leconte, R. Rizk, F. Gourbilleau, P. Voivenel, M. Lejeune, C. Goncalves, Solid State Phenom. 80–81 (2001) 65.
[5] A. Matsuda, T. Goto, Mater. Res. Soc. Symp. Proc. 164 (1990) 3.
[6] A. Matsuda, Thin Solid Films 337 (1999) 1.
[7] S. Veprek, M. Heintze, F.A. Sarott, M. Jurcik-Rajman, P. Willmott, Mater. Res. Soc. Proc. 118 (1988) 3.
[8] I. Shimizu, J. Hanna, H. Shirai, Mater. Res. Soc. Symp. Proc. 164 (1990) 195.
[9] L. Lutterotti, H.-R. Wenk, S. Matthies, in: J.A. Szpunar (Ed.), Textures of Materials, 2, NRC Research Press, Ottawa, 1999, pp. 1599–1604.
[10] S. Matthies, G.W. Vinel, Phys. Status Solidi B 112 (1982) K111.
[11] J.J. Heizmann, C. Laruelle, J. Appl. Crystallogr. 19 (1986) 467.
[12] http://pcb4122.univ-lemans.fr/powdif/low_fwhm_and_rp.html#t4B.
[13] N.C. Popa, J. Appl. Crystallogr. 31 (1998) 176.
[14] M. Morales, D. Chateigner, L. Lutterotti, J. Ricote, Mater. Sci. Forum 408–412 (2002) 113.
[15] S. Matthies, G.W. Vinel, K. Helming, Standard Distributions in: Texture Analysis, 1, Akademie-Verlag, Berlin, 1987, 449 pp.
[16] H.-J. Bunge, Transactions, in: P.R. Morris (Ed.), Texture Analysis in Materials Science, Butterworths, London, 1982.
[17] GOMAN, INEL France SA Licence 1997; POFINT: 'Pole figure interpretation', CNRS-INEL France SA Licence 2002.
[18] H.-R. Wenk, S. Matthies, J. Donavan, D. Chateigner, J. Appl. Crystallogr. 31 (1998) 262.
[19] Y. Leconte, P. Marie, X. Portier, M. Lejeune, R. Rizk, Thin Solid Films 427 (2003) 252.
[20] D. Chateigner, F. Brunet, A. Deneuville, P. Germi, M. Pernet, P. Gonon, J. Cryst. Growth 148 (1995) 110.